Enhanced Heat Transfer from Arrays of Jets Impinging on Plates

J. Badra, A. R. Masri, M. Freeman, and M. Fitch*

School of Aerospace, Mechanical, and Mechatronic Engineering
The University of Sydney
*Fitch Milley Engineering Pty, Ltd, Willoughby NSW 2068

Abstract

Multiple jets of various shapes, orientation and configuration are used regularly in a wide range of engineering applications to provide heating or cooling with impingement on a plate being one of the most common configurations due to the improved heat transfer rates. Design optimization has largely relied on empirical correlations that are limited by the range over which they were originally generated. Computational Fluid Mechanics is now sufficiently advanced to be used as an alternative method for obtaining optimal designs.

This project uses the commercial Fluent package to compute heat transfer from a bank of jets impinging on a plate. Results for a single jet are validated against experimental data. The use of advanced turbulence modeling and appropriate boundary layer formulations are key ingredients for obtaining reliable calculations. The heat transfer resulting form the use of multi-jet configurations will be discussed in the paper.

Nomenclature

D	nozzle diameter, m
h	local heat transfer coefficient, w/m^2k
$\bar{h}$	average heat transfer coefficient, w/m^2k
k	thermal conductivity of air, $w/m\ k$
H	distance between nozzle exit and impinging plate, m
H/D	dimensionless jet-to plate-spacing
Nu	local Nusselt number
$\overline{Nu}$	average Nusselt number
I	turbulent intensity
x_n	jets spacing, m
q	combined convective and radiative heat flux
R	radial distance from stagnation point, m
R/D	dimensionless radial distance
Re	Reynolds number based on the exit diameter, $= UD\rho/\mu$
U	mean velocity at jet exit, m/s
ρ	density of air, Kg/m^3
μ	kinetic viscosity of air, $Kg/m \cdot s$
T	temperature, K or $°C$
ΔT	temperature difference, K or $°C$

Subscript

a	ambient
w	wall
j	jet
ref	reference
$3D$	three-dimensional

Introduction

Impinging jets are used in many engineering applications to enhance heat transfer for cooling or heating purposes or mass transfer for vapour deposition. Typical heat transfer applications include electronics cooling, paper drying, metal annealing and sheet metal treatment. In most of these applications, arrays of jets are used in a range of configurations and shapes with the objective on optimizing heat transfer rates. However, the flow and geometry parameters that interact and affect the heat transfer rates are numerous hence complicating the optimization process particularly when this is to be achieved experimentally.

Computational Fluid Dynamics (CFD) has advanced sufficiently to enable such heat transfer calculations to be made and potentially with good confidence levels. The accuracy of the calculations depend on a number of parameters including the choice of turbulence model and the treatment of the boundary layer since this largely dictates the nature of the heat transfer. Calculations of heat transfer from single impinging jets have been made by Behnia et al. [1999] using the $v^2 - f$ turbulence model and the results compared reasonable well with measurements of [1, 2, 6, 19, 28].

The simple case of a single impinging jet, shown schematically in Fig. 1, has been widely studied both experimentally and numerically and hence forms a good platform for model validation. The flow field of an impinging jet configuration has three distinctive flow regions namely free jet region, a deflection region (or stagnation region) and a wall jet region. The velocity difference between the potential core of the jet and the ambient fluid creates a shear layer. The mean shear strain is zero in the free jet region and the production of kinetic energy is exclusively due to the normal straining. As the flow approaches the wall, the centerline velocity decays until it reaches zero at the stagnation point. The proximity of the solid boundary causes the deflection of the jet and a strong streamline curvature region is observed. Downstream the stagnation point, a wall jet evolves along the wall. Turbulence energy is increased due to the mean shear strain which dominates in the near wall region.

Despite its simplicity, this flow has some heat transfer features that are not easy to predict. The distance of the jet exit plane from the wall or plate is a key controlling parameter. When this distance is larger than the potential core, measurements have

shown [1, 2, 3, 4, 6, 17, 19, and 28] that the Nusselt number decreases monotonically with increasing radial distance away from the jet axis. However, with closer distances, a double peak in Nusselt number develops with the first one forming close to the centreline and the second one at larger radial distances. The magnitude of the peaks becomes more distinct at higher jet Reynolds numbers. A possible explanation for this behaviour is that when the jet inlet to wall distance is smaller than the potential core, there will not be sufficient time for mixing with the surrounding fluid. Thus the flow in the vicinity of the stagnation point has a low turbulent intensity and hence a lower Nusselt number (Nu) for H/D<5. This feature is not easy to reproduce and forms a good test for the robustness of the turbulence model used in the calculations. Behnia et al. [1999] have reproduced such behaviour numerically only with the $v^2 - f$ turbulence model.
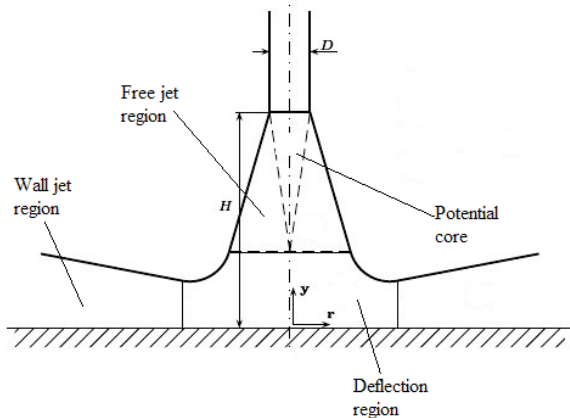

Figure 1. Jet impingement configuration.

With arrays of jets, the situation if much more complex due to the multitude of additional parameters that affect the fluid dynamics and the heat transfer rates. Interactions between adjacent jets also become and issue hence imposing more severe requirements on the computations. Reliable measurements of heat transfer from multiple impinging jets are not abundant and the data provided by Goldstein and Timmers (1982) is extremely useful as it forms a good platform for model validation.

The objective of this paper is to demonstrate that accurate heat transfer calculations can be obtained from single and multiple jets using the SST $k - \omega$ turbulence model. Such calculations are validated against experimental data from Lee et al. (1999) and Goldstein and Timmers (1982). The complex heat transfer features associated with both flow configurations are faithfully reproduced using the model. The longer term objective of this research is to optimize the heat transfer rates by optimizing the layout of array of impinging jets with respect to the plate.

Numerical procedure
The FLUENT-6.3.26 commercial package is used here to perform three-dimensional calculations for both single and multiple jets impinging on a plate. The flow and turbulent fields have to be accurately solved to obtain reasonable heat transfer predictions. Second order scheme is used for all terms that affect heat transfer. Second order discretization scheme is used for the pressure; second order upwind discretization scheme is used for momentum,

turbulent kinetic energy, specific dissipation rate, and the energy. Flow, turbulence, and energy equations have been solved. The standard SIMPLE algorithm is adopted for the pressure-velocity coupling. Grid independent solutions are obtained for all the flow configurations presented here.

To be consistent in comparing with the experimental data the velocity profile at the exit of the jet should be fully developed. This can be done by using fully developed turbulent velocity profile as a boundary profile file and than use this profile file to describe the inlet jet velocity. The inlet of the jet is two pipe diameters upstream of the jet exit, so the pipe flow profile may evolve in the nozzle as the flow is approaching the jet exit.

Single impinging jet
The examined domain consists of quarter of the whole domain with two symmetry planes, which is more time efficient and due to limits of computational resources. Details about the geometry, material used and boundary conditions are shown in Tables 1, 2 and Figure 2.

Properties	Values
D	$25mm$
H	$50,200,300mm$
Re	$5,000 - 30,000$
T_j	$20°c$
T_w	$40°c$

Table 1. Geometrical and flow details.

Properties	Incompressible ideal gas Air
ρ	$1.20147m^3/kg$
k	$0.0242w/m.k$
μ	1.7894×10^{-5}
Ratio of specific heats	1.4

Table 2. Material properties.

The boundary conditions are imposed based on the experimental conditions (temperature and velocity of the impinging jet, temperature of the ambient air and the temperature of the plate).
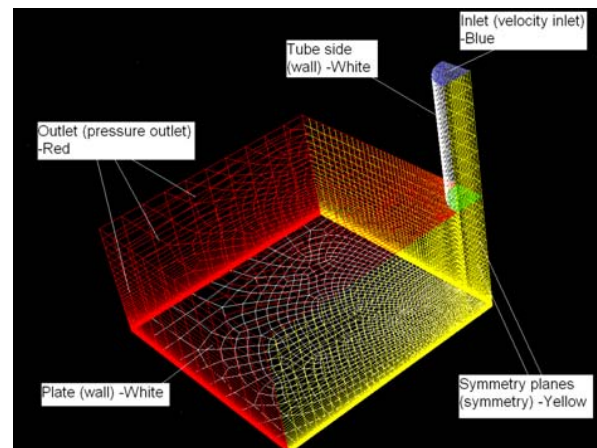

Figure 2. The numerical domain (*H/D=2*) and its boundary conditions.

Turbulence model

The turbulent models available in Fluent 6.3.26 are models based on the Reynolds Averaged Navier-Stokes Equations for 2D or 3D domains. In the present study, six different turbulent models are tested and compared in some cases. The turbulent models used in this numerical analysis are: (i) Standard $k - \varepsilon$ model, (ii) RNG $k - \varepsilon$ model, (iii) Realizable $k - \varepsilon$ model, (iv) Standard $k - \omega$ model, (v) SST $k - \varepsilon$ model and (vi) the Reynolds Stress model (RSM). These are now widely available tools where the governing equations and the derivation details are outlined extensively elsewhere [26] and will not be reproduced here.

Special care has been taken for the wall function used. The $k - \varepsilon$ and RSM family have the option to use Enhanced Wall Treatment (EWT). In this paper, EWT has been used for $k - \varepsilon$ and RSM. EWT combines a blended law-of-the wall and a two-layer zonal model. It is suitable for low-Re flows or flows with complex near-wall phenomena. Using EWT as an option for the turbulent models mentioned before will modify those turbulence models for the inner layer. EWT generally requires a fine near-wall mesh capable of resolving the viscous sub-layer (at least 10 cells within the "inner layer"). The mesh near the wall is refined enough to make $y^+ \approx 1$. The $k - \omega$ family of models do not have the options of using enhanced wall treatment but SST $k - \omega$ Combines the original Wilcox model for use near walls and the standard $k - \varepsilon$ model away from the walls using blending function.

Choice of T_{ref}

Not enough information is given about those experiments to do valuable comparison of numerical data with the available experimental data. The data from [17] can be reproduced numerically because all the details are known especially the difference in temperature between the jet and the plate (ΔT). This parameter has to be known if a valid comparison between experimental and the calculations is to be done. Numerically, the process followed to calculate the local and average Nusselt number passing through the total heat flux at the surface involves the local (h) and average heat transfer coefficient ($\bar{h}$), the jet diameter (D), and basically the difference in temperature between the jet and surface (ΔT). The following equations is used to obtain the surface heat transfer coefficient,

$$ h_{eff} = \frac{q}{T_w - T_{ref}} $$

(1)

Where q is the combined convective and radiative heat flux, T_w is the wall temperature, and T_{ref} is the reference temperature defined in the reference values panel available in Fluent. T_{ref} is a constant value that should be representative of the problem. Its unit quantity is the heat-transfer- coefficient. The radiative heat flux is neglected here because it is not considered in the experiment, where its uncertainty ranged from 0.6% to 2.3%.

There are two method for defining T_{ref}. It can be the local adiabatic wall temperature as it was used by Gardon and

Cobonque (1961) and Goldestein et al. (1986) or it can be the jet exit temperature. The warming and cooling effects of the jet due to thermal entrainment of ambient air were minimized by maintaining the impinging air jet temperature close to ambient temperature for all experiments $T_a - T_j = \pm 0.1 °C$. In present study, the jet exit temperature was used to calculate the local heat transfer coefficient instead of the local adiabatic wall temperature. Note that the temperature of the plate is kept constant. It means that the thermal boundary condition of the plate will be constant temperature. The surface Nusselt number is then calculated using the following equation,

$$ Nu = \frac{h_{eff} L_{eff}}{k} $$

(2)

Where h_{ref} is the heat transfer coefficient, L_{ref} is the reference length defined in Fluent, and k is the molecular thermal conductivity of air or gas coming from the jet.

Model validation

Computations were first performed for the particular case mentioned experimentally in [17]. The details of the computational domain are shown in Table 1, 2 and Figure 4. The first case was done for $H / D = 6$. The Reynolds number is chosen to be 25,000 because it is validated against data from Baughn (1989). Figure 3 shows the Nusselt number distribution using various turbulent models. The features of the experimental and numerical simulations are the same. The local Nusselt number peaks at the stagnation region, and then it decreases monotonically upon going outward along the impingement plate.
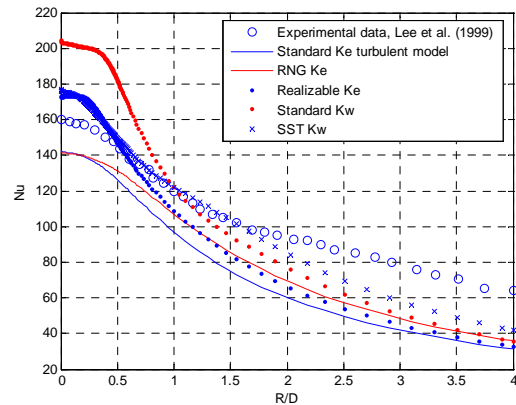

Figure 3. Simulated Nusselt number distribution for the impinging jet on the flat plate at *H/D*=6 and Re=25,000.

As can be noticed the experimental stagnation Nusselt number for this case is 160 and the numerical ones range from 140 to 203. The best that describes the stagnation Nusselt number are the SST $k - \varepsilon$ and the Realizable $k - \varepsilon$ models.

Analysis on the average Nusselt number has been done. The numerical results are compared with empirical correlation done for the special experimental case. The least-square estimations of the average Nusselt number are evaluated at the locations of *R/D* =2 and 4 for the nozzle-to-plate spacings of $2 \le H / D \le 10$ and the jet

Reynolds number ranged from 5,000 to 30,000. The least-square fittings have the following correlations [17]:

$$\overline{Nu}_{R/D=0\to2} = 0.203\,\mathrm{Re}^{0.635}\left(\frac{H}{D}\right)^{-0.0968}$$

(3)

And

$$\overline{Nu}_{R/D=0\to4} = 0.083\,\mathrm{Re}^{0.708}\left(\frac{H}{D}\right)^{-0.144}$$

(4)

	R/D=0→2	Error (%)		R/D=0→4	Error (%)
Correlation	105.9			83.3	
Standard $k-\varepsilon$	94.8	10.5		57.7	30.7
RNG $k-\varepsilon$	94.5	10.7		57.5	30.9
Realizable $k-\varepsilon$	95.6	9.7		57.3	31.2
Standard $k-\omega$	109.3	3.2		65	21.9
SST $k-\omega$	110.9	4.7		70.9	14.8

Table 3. Average Nusselt number for *R/D*=0→2 and 4 against correlation data.

The model that describes well the average Nusselt number is the SST $k-\omega$ model. The second numerical case is the model with *H/D*=2. This case has been validated as well. The Reynolds number is 15,000.
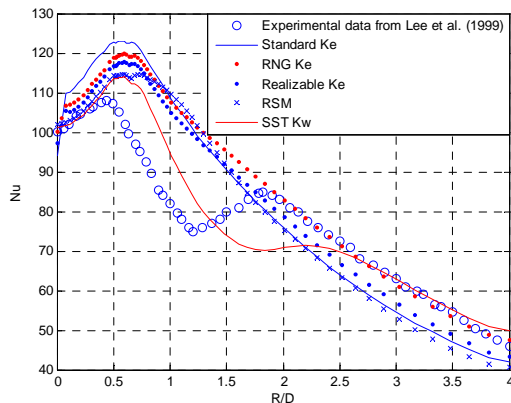
Figure 4. Simulated Nusselt number distribution for the impinging jet on the flat plate at *H/D*=2 and Re=15,000.

The flow geometry in this case is complicated compared with the high jet-to-plate distance case. The corresponding heat transfer characteristics are very complicated due to complex interaction between the jet and the impingement plate. It has been proved that the Nusselt number peaks two times for *H/D*=2. The local Nusselt number increases from a local minimum at the stagnation point to the first peak and then decreases rapidly and again

increases along the wall, giving the second peak in transition region. This case has been simulated numerically and results of using several turbulent models are show in Figure 4.

The only model that successfully targeted and described the features of this low *H/D* case is the SST $k-\omega$. The first peak appears at $R/D \approx 0.5$ and the second peak is at $R/D \approx 2$, it is almost the same locations as mentioned in the experimental data. SST $k-\omega$ agrees quantitatively with the experiment. More tests have been done using SST $k-\omega$ model but now to check the effect of Reynolds number on the distribution of the local Nusselt number and the behaviour of the first and second peaks. Figure 5 shows the distribution of the Nusselt number for different Reynolds numbers using the same turbulent model.
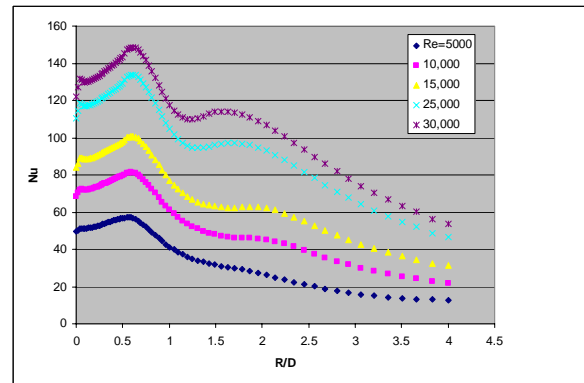
Figure 5. Variations of local Nusselt numbers for *H/D*=2 for different Reynolds numbers.

As can be observed the first peak is moving outward the stagnation point as the Reynolds number increases. This is mentioned in the experimental data. The second peak becomes more clear and obvious as the Reynolds number increases. This is mentioned as well in the experiment. Quantitatively SST $k-\omega$ is very good. An error of just 2.3% has been got for the average Nusselt number at *R/D*=2 and Reynolds number of 15,000 between numerical and correlation data. Another test has been done by fixing the Reynolds number at 15,000 and changing *H/D* between 2 and 6 using SST $k-\omega$ turbulent model and the results are shown in Figure 6.
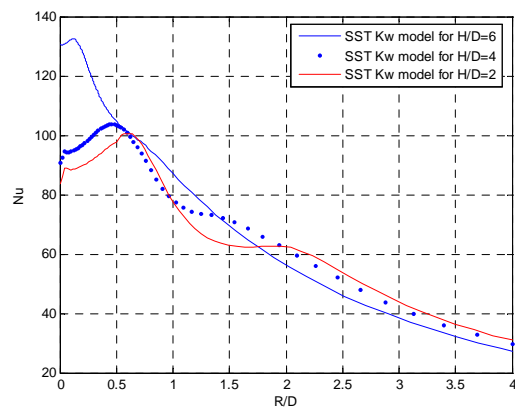
Figure 6. Variations of local Nusselt numbers for Re=15,000 and different *H/D*.

The first and second peaks are moving toward the stagnation point as *H/D* increases until they reach *H/D*=6 so they disappear, which is the real case. The stagnation Nusselt number is maximum at *H/D*=6. This has been proved by many researchers [17, 20. etc…].

Array of jets
Most of the industrial and engineering applications involve arrays of jet or slot nozzles. However, limited experimental are available despite the common use of his configuration. Goldstein and Timmers (1982) have performed an experimental study for two kinds of arrays. The first is three jets in a row with jet-to-plate spacing of six and two diameters. The second is an array of a single jet surrounded by a (hexagonal) set of six jets. The diameter of the jets is 10mm, the spacing between the jets is four diameters, and the Reynolds number is equal to 40,000. The difference in temperature between the jets and plate enables us make qualitative comparison between experimental and numerical data. The three co-linear jets with *H/D* = 6 case has been taken as the reference of comparing the numerical data. The 3D domain shown in Fig. 7 is an adequate reproduction of the experimental condition showing six circular jets with for *H/D*=6.
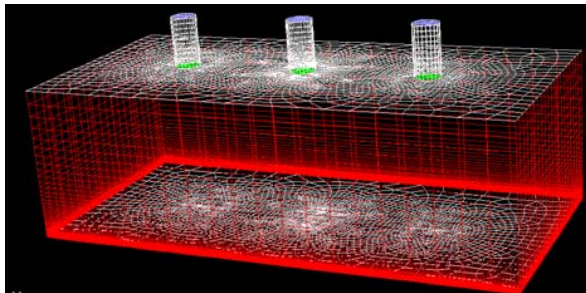

Figure 7. Multi-jet domain with *H/D*=6.

The mesh shown in Fig. 7 consists of 186,040 cells and this corresponds to a grid independent solution. The computed domain is quarter of the shown domain in Fig.7 and again special care has been taken for near wall treatment and the wall y^+ values are less than 1. The time needed for a converged solution is 3 hours and 15 minutes on a 2.40Ghz CPU and 1.00 GB of Ram computer.

Figure 8 shows Nusselt number contours for the three co-linear nozzles and these are qualitatively similar to those presented by Goldstein and Timmers (1982). The contours of the middle jet are compressed by interaction with the outer jets contours. Maximum local Nusselt numbers are located under jets.
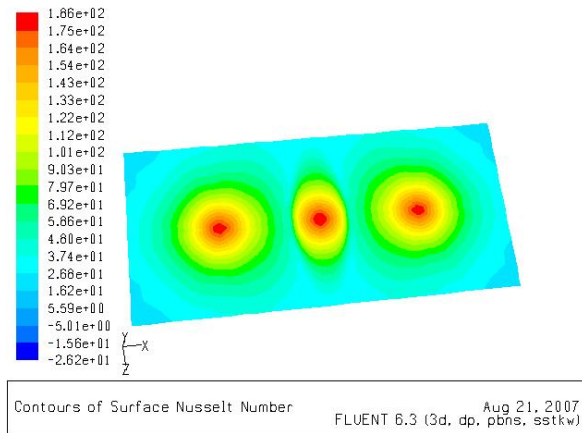

Figure 8. Nusselt number contours for multi-jet case with *H/D*=6.

Figure 9 shows the local Nusselt numbers computed along a line parallel to the axis joining the jet centrelines. Also shown on the Figure are the measurements reported by Goldstein and Timmers (1982) for the same configuration. As can be noticed from Figure 9 the local Nusselt number distribution near the jets axis are very close and nearly lie above each other and away from the stagnation point of each jet the difference between experimental and numerical data increases as it was mentioned for single jet case at *H/D*=6.
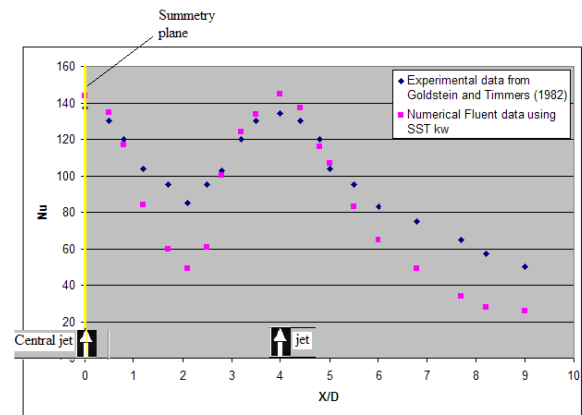

Figure 9. Nusselt number on surface along line through geometric centres of the 3 co-linear impinging jets.

No local maximum Nusselt numbers are observed between the jets because *H/D* is high. This is mentioned in the experimental results of Goldstein and Timmers (1982).

Conclusions
In this study, numerical simulation using the commercial package Fluent and Gambit has been validated against experimental data. Many turbulent models have been used. The SST $k - \omega$ model showed that it can describe that kind of problems the best. The second peak in Nusselt number at low jet-to-plate distances was well predicted by only the SST $k - \omega$ model. This model has been used to evaluate the influence of jet-to-plate distance, Reynolds number, and multi-jet case. SST $k - \omega$ was shown to perform very well in a range of *H/D* and Re, in order to give confidence in its use as a predictive tool.

Multi-jet case has been done and evaluated against experimental data as well. It showed very good qualitative agreement with the available data set.

References

[1] Baughn, J., Hechanova, A. & Yan, x., An Experimental Study of Entrainment Effects on the Heat Transfer From a Flat Surface to a Heated Circular Impinging Jet, *ASME J. Heat Transfer*, 113, 1991, 1023-1025.

[2] Baughn, J. & Shimizu, S., Heat Transfer Measurements from a Surface with Uniform Heat Flux And an Impinging Jet, *ASME J. Heat Transfer*, 111, 1989, 1096-1098.

[3] Benhia, M., Ooi, A. & Gregory, P., Prediction of Turbulent Heat Transfer in Impinging Jet Geometries, *Modeling and Simulation of Turbulent Heat Transfer*, 16, 2006, 147-175.

[4] Behnia, M., Parneix, S., Shabany, Y. & Durbin, P. A., Numerical study of Turbulent Heat Transfer in Confined and Unconfined Impinging Jets, *Int. J. Heat Mass Transfer*, 20, 1999, 1-9

[5] Buchlin, J. M., Gouriet, J. B., Planquart, P., Van Beek, J. & Renard, M., Experimental and Numerical Study of Convective Heat Transfer in an Arrays of Slot Jets, ASME Proceedings, 2002.

[6] Colucci, D. & Viskanta, R., Effect of Nozzle Geometry on Local Convective Heat Transfer to a Confined Impinging Air Jet, Experimental Thermal and Fluid Science, 13, 1996, 71-80.

[7] Coussirat, M., Van Beek, J., Mestres, M., Egusguiza, E., Buchlin, J. –M. & Escaler, X., Computational Fluid Dynamics Modeling of Impinging Gas-Jet Systems: I. Assessment of Eddy Viscosity Models, *Journal of Fluids Engineering*, 127, 2005, 691-703.

[8] Craft, T. J., Graham, L. J. W. & Launder, B. E., Impinging Jet Studies for Turbulence Model Assessment- II. An Examination of the Performance of Four Turbulence Models, *Int. J. Heat and Mass Transfer*, 36, 1993, 2685-2697.

[9] Gardon, R. & Akfirat, J. C., Heat Transfer Characteristics of Impinging Two-Dimensional Air Jets, ASME, *Journal of Heat Transfer*, 88, 1966, 101-107.

[10] Gardon, R. & Cobonque, J., Heat Transfer between a Flat Plate and Jets of Air Impinging on It, Part III, International Heat Transfer Conference Proceedings, 1961, 454-460.

[11] Goldstein, R. J., Behbahani, A. I. & Heppelmann, K. K., Streamwise Distribution of the Recovery Factor and the Local Heat Transfer Coefficient to an Impinging Circular Air Jet, *Int. J. Heat Mass Transfer*, 29, 1986, 1227-1235.

[12] Goldstein, R. J. & Timmers, J. F., Visualization of Heat Transfer From Arrays of Impinging Jets, *Int. J. Heat Mass Transfer*, 25, 1982, 1857-1982.

[13] Gupta, A. & Irannezhed, M., Prediction of Axisymmetric impinging jet, MTF112 report, Convective Heat Transfer, 2005, Chalmers, Sweden.

[14] Hofman, H., Martin, H. & Kind, M., Numerical Simulation of Heat Transfer from an Impinging Jet to a Flat Plate, *Chem. Eng. Technol.*, 27, 2004, 27-30.

[15] Jambunathan, K., Lai, E., Moss, M. A. & Button, B. L., A Review of Heat Transfer Data for Single Circular Jet Impingement, *Int. J. Heat and Fluid Flow*, 13, 1992, 106-115.

[16] Kroger, M., & Krizek, F., Mass-Transfer coefficient in Impingement Flow from Slotted Nozzles, *Int. J. Heat Mass Transfer*, 9, 1966, 337-344.

[17] Lee, J. & Lee, S. J., Stagnation Region Heat Transfer of a Turbulent Axisymmetric Jet Impingement, *Experimental Heat Transfer*, 12, 1999, 137-156.

[18] Lou, Z. Q., Mujumdar, A. S. & Yap, C., Effects of Geometric Parameters on Confined Impinging Jet Heat Transfer, *Applied Thermal Engineering*, 25, 2005, 2687-2697.

[19] Lytle, D. & Webb, B., air Jet Impingement Heat Transfer at Low Nozzle-Plate Spacings, *Int. J. Heat Mass Transfer*, 37, 1994, 1687-1697.

[20] Martin, H., Heat and Mass Transfer between Gas Jets and Solid Surfaces, *Advances in Heat Transfer*, 13, 1977, 1-60.

[21] Moris, G.K., Garimella, S.V. & Fitzgerald, J. A., Improved Predictions of the Flow Field in Submerged and Confined Impinging Jets Using the Reynolds Stress Model, Intersociety Conference on Thermal Phenomena, 1998, 362-370.

[22] Nguyen, A. & Evans, G., computational Fluid Dynamics Modeling of Gas Jets Impinging onto Liquid Pools, Third International Conference on CFD in the Minerals and Process Industries, 2003, 71-76.

[23] Nitin, N. & Karwe, M. V., Numerical Simulation and Experimental Investigations of Conjugate Heat Transfer between a Turbulent Hot Air Jet Impinging on a Cookie-Shaped Object, *Journal of Food science*, 69, 2004, 59-65.

[24] Rundstorm, D. & Moshfegh, B., Investigations of Flow and Heat Transfer of an Impinging Jet in a Cross-Flow for Cooling of a Heated Cube, Itherm 2004- Ninth intersociety Conference on Thermal and Thermomechanical Phenomena in Electronic Systems, 1, 2004, 455-462.

[25] Salamah, S. A. & Kaminski, D. A., Modeling of turbulent Heat Transfer from an Array of Submerged Jets Impinging on a Solid Surface, *Numerical Heat Transfer*, 48, 2005, 315-337.

[26] User's Guide Manual, Fluent 6.3 Documentation, Ansys.

[27] Worth, N. A. & Yang, Z., Simulation of an Impinging Jet in a Crossflow Using a Reynolds Stress Transport Model, *Int. J. Numer. Meth. Fluids*, 52, 2006, 199-211.

[28] Yan, X., A Preheated-Wall Transient Method Using Liquid Crystals for the Measurement of Heat Transfer on External Surfaces and in Ducts, Ph. D. Thesis, 1993, University of California, Davis.

[29] Yan, X., Baughn, J. W. & Mesbah, M., The Effect of Reynolds Number of the Heat Transfer Distribution from a Flat Plate to an Impinging Jet, Fundamental and Applied Heat Transfer Research For Gas Turbine Engines, ASME, HTd-Vol. 226, 1992, 1-7.

[30] Zhao, W., Kumar, K. & Mujumdar, A. S., Flow and Heat Transfer Characteristics of Confined Noncircular Turbulent Impinging Jets, Drying Technology, 22, 2004, 2027-2049.